Numerical Implementation and Performance of Perfectly Matched Layer Boundary Condition for Waveguide Structures

Zhonghua Wu and Jiayuan Fang, *Member, IEEE*

Abstract—**This paper presents some numerical implementation issues and the performance of Berenger's perfectly matched layer (PML) boundary condition for modeling wave propagation in waveguide structures by the finite-difference time-domain (FDTD) method. The relation between the thickness and the conductivity profile of the perfectly matched layer is studied and a guideline for the selection of PML parameters is given. It is shown that the standard Yee's time-marching scheme results in virtually the same numerical solution as the exponential time-marching scheme. Numerical tests are provided for parallel-plate and rectangular waveguides and microstrip lines. It is found that PML is very effective in absorbing TEM and quasi–TEM waves, as well as nonTEM waves somewhat above cutoff frequencies, but ineffective in absorbing evanescent waves and nonTEM waves near cutoff frequencies. The reason for the ineffectiveness of PML for absorbing evanescent waves is explained. Comparative study of PML and Higdon's boundary condition shows that high-order Higdon's boundary condition can reach the same performance of 16-cell PML and can be adjusted for absorbing evanescent waves, but PML is in general more robust to implement. Performance of the boundary condition obtained by combining PML and Higdon's boundary condition is evaluated.**

I. Introduction

THE PERFECTLY matched layer (PML), recently proposed by Berenger, is an artificial lossy material used for the truncation of numerical computation domains in applying the finite-difference time-domain method [1], [2]. The performance of PML, reported in [1], [2], appears to be overwhelmingly superior to other available absorbing boundary conditions. Several papers have also appeared, soon after Berenger's invention, that verified the method of PML and successfully implemented PML in many applications [3],]4].

This paper presents a detailed study of the performance of PML as it is applied to model wave propagation in waveguide structures used in microwave and digital circuit interconnects. Unlike situations in most scattering problems, evanescent waves are frequently encountered in waveguide structures. While some positive results on PML for evanescent waves in waveguides have recently been reported [4], the analytic field solution in PML, as presented by Berenger [1], implies that PML shouldn't work for evanescent waves.

Manuscript received February 15, 1995; revised August 29, 1995. This work was supported in part by the National Science Foundation Contract MIP-9357561 and the Integrated Electronics Engineering Research Center (IEEC) at the State University of New York at Binghamton.

The authors are with the Department of Electrical Engineering, State University of New York at Binghamton, Binghamton, NY 13902 USA.

IEEE Log Number 9415558.

Our numerical tests show that PML is indeed very effective in absorbing TEM and quasi–TEM waves, as well as nonTEM waves somewhat above cutoff frequencies. These numerical tests also confirm that PML is ineffective in absorbing evanescent waves and nonTEM waves near cutoff frequencies.

This paper begins with a discussion on the wave propagation in PML and on numerical implementation of PML. The mechanism of how PML absorbs propagating waves but not evanescent waves is explained. A relation between the thickness and the conductivity profile of the perfectly matched layer is provided as a guideline for implementing PML. The performance of the standard Yee's time-marching scheme is compared with the exponential time-marching scheme used by Berenger [1],]2]. Section III presents the performance of PML for parallel-plate and rectangular waveguides. Analytic predictions on behaviors of propagating and evanescent waves in waveguides filled with PML are compared with numerically computed results. Comparisons are made between PML and high order Higdon's type of boundary conditions. The performance of the boundary condition resulted from combining PML and Higdon's type of boundary condition is evaluated. Effects of PML in modeling wave propagation in microstrip lines are presented in Section IV.

II. Wave Propagation in PML and Numerical Implementation Issues

With the PML technique introduced by Berenger, the six components of the electromagnetic field are split into 12 subcomponents, and the six scalar Maxwell's equations are replaced by 12 scalar equations. The PML medium has both electric and magnetic losses. By properly associating different electric or magnetic conductivities to different subcomponents, Berenger showed that PML theoretically would not cause any reflection at an interface with the free-space for incident fields of any frequencies and incident angles. Detailed formulations of PML can be found in [1]–[3] and are not to be repeated here.

A. Wave Propagation in PML

Let us take a 2–D example for illustration. Suppose, in the x-y plane, a semi-infinite PML medium is interfaced with a semi-infinite free space at the surface $x = 0$. The PML is in the region $x > 0$. Based on the criteria described by Berenger for determining the electric and magnetic losses in PML [1], the electric and magnetic conductivities, σ_y and σ_y^*, should be

zero; and the electric and magnetic conductivities, σ_x and σ_x^*, should satisfy the condition

$$\sigma_x/\epsilon_0 = \sigma_x^*/\mu_0. \tag{1}$$

Consider an incident field in the free space

$$\psi = \psi_0 e^{j\omega\left(t-\frac{x\cos\varphi+y\sin\varphi}{c}\right)} \tag{2}$$

where ψ represents any component of the field, ψ_0 is its amplitude, c is the speed of light, and φ is the angle between the x axis and the direction of the wavenumber vector. Berenger showed that the field component ψ, after entering the PML medium, could be expressed as [1]

$$\psi = \psi_0 e^{j\omega\left(t-\frac{x\cos\varphi+y\sin\varphi}{c}\right)} e^{-\frac{\sigma_x\cos\varphi}{\epsilon_0 c}x}. \tag{3}$$

Next, let us have a close examination of (3) to see how a wave propagates in PML. If in the x direction the field is propagating, then $\cos\varphi$ is a real number, and the term $e^{-\frac{\sigma_x\cos\varphi}{\epsilon_0 c}x}$ in (3) contributes to the attenuation of the field. The smaller the angle φ, the larger the attenuation. When the angle φ reaches 90°, there will be no attenuation of the wave in PML. On the other hand, if the variation of the field in the x direction is of evanescent nature, $\cos\varphi$ will be an imaginary number, and the term $e^{-\frac{\sigma_x\cos\varphi}{\epsilon_0 c}x}$ no longer decays the field in the x direction. In this case, the presence of the PML does not add any additional attenuation of the wave beyond the original attenuation (due to the term $e^{-j\frac{\omega\cos\varphi}{c}x}$) of the evanescent wave itself.

From the properties of the wave propagation in PML discussed above, one can predict that, in the modeling of wave propagation in waveguide structures, PML can be effective for waves somewhat above cutoff frequencies, but ineffective for waves near cutoff frequencies (when $\cos\varphi$ is close to zero) and evanescent waves (when $\cos\varphi$ is an imaginary number). Numerical tests presented in later sections of this paper confirm this prediction.

B. Selection of PML Parameters

In actual numerical computations, the thickness of PML is finite, and the PML is terminated by a boundary, say, an electric wall. As the wave in PML reaches the terminating boundary and gets reflected, it is further attenuated as it propagates back toward the free space—PML interface. The remaining part of this backward propagated wave at the free space—PML interface will pass through the interface and enter the free-space region as an unwanted reflection wave. By adjusting the value of conductivity, one can control the amount of attenuation in PML, i.e., the amount of reflection from PML.

The free space—PML interface has theoretically no reflection to incident fields of any frequencies and incident angles. For any thickness of PML, ideally one can choose σ's to be sufficiently large to make reflection from PML as small as wanted. However, this is not the case in actual numerical computations. Any discontinuities in material properties, such as the conductivity σ, will cause numerical reflections. Therefore it is of advantage to have conductivity σ vary continuously

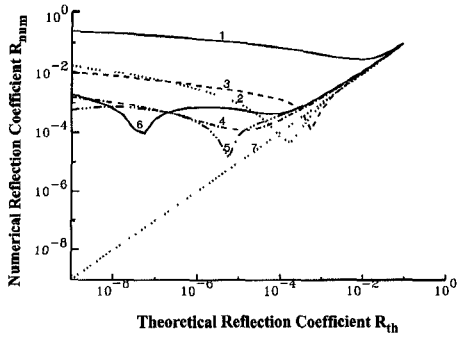

Fig. 1. Numerical reflection coefficient versus theoretical reflection coefficient at the normal incident angle for 4-cell PML of different conductivity profiles. Curves 1–6 correspond to n in (4) be chosen as 0, 0.5, 1, 1.5, 2, and 2.5. Curve 7 is a line on which the numerical reflection coefficient equals the theoretical one.

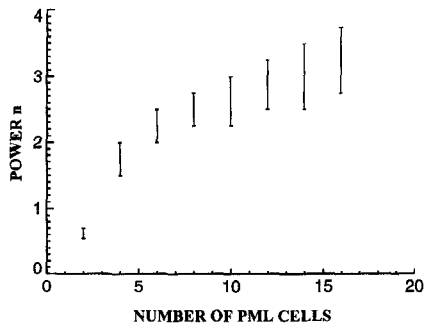

Fig. 2. Optimum range of the value n in (4) for different thicknesses of PML.

with space, as done by Berenger [1]. That is, let σ increase from zero at the free space—PML interface to its maximum value σ_m at the outer side of the PML gradually. Let the thickness of PML be denoted as δ, the conductivity σ can take the following form

$$\sigma(x) = \sigma_m\left(\frac{x}{\delta}\right)^n. \tag{4}$$

Then, for PML terminated by an electric wall, the theoretical reflection coefficient $R_{\rm th}$, when the reflection due to the spatial variation of conductivity is ignored, can be calculated as

$$\begin{aligned} R_{\rm th}(\varphi) &= e^{-2\frac{\cos\varphi}{\epsilon_0 c}\int_0^\delta \sigma(x)dx} \\ &= e^{-\frac{2}{n+1}\frac{\sigma_m\delta}{\epsilon_0 c}\cos\varphi}. \end{aligned} \tag{5}$$

From the theoretical reflection coefficient $R_{\rm th}$ at the normal incidence ($\varphi = 0$) and the power n, the maximum value of the conductivity σ_m can be found as

$$\sigma_m = -\frac{(n+1)\epsilon_0 c}{2\delta}\ln R_{\rm th}. \tag{6}$$

The actual reflection coefficient in the numerical computation, denoted as $R_{\rm num}$, is somewhat different from the theoretical one. If the theoretical reflection coefficient $R_{\rm th}$ is set to be too small, then the abrupt change of σ with space can result in a large reflection in the numerical computation. Therefore, the value of $R_{\rm th}$ as well as the power n need to be properly chosen to achieve small reflections. Fig. 1 shows the numerical reflection coefficient $R_{\rm num}$, obtained

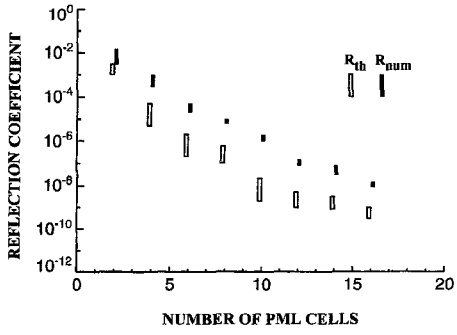

Fig. 3. Optimum range of theoretical reflection coefficients as well as the corresponding achievable numerical reflection coefficients at the normal incident angle for different thicknesses of PML.

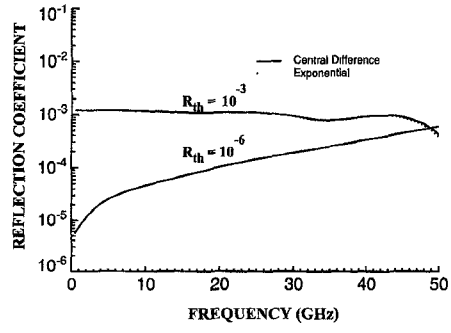

Fig. 4. Comparison between reflection coefficients of an 8-cell PML implemented with the central difference and exponential time-marching schemes.

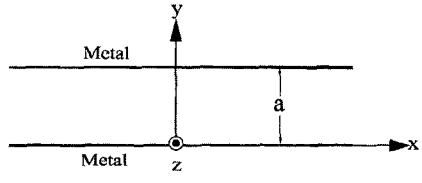

Fig. 5. Cross section of a parallel-plate waveguide ($a = 40$ mm).

from numerical computations, versus the theoretical reflection coefficient $R_{\rm th}$ at the normal incident angle for 4-cell thick PML. Curves 1–6 in Fig. 1 correspond to the power n chosen to be 0, 0.5, 1, 1.5, 2, and 2.5, respectively. Curve 7 is a reference line on which the numerical reflection coefficient equals the theoretical one. From Fig. 1, it can be seen that the optimum values of $R_{\rm th}$ and n are somewhat fuzzy to determine. However, one can obtain a range of $R_{\rm th}$ and n, within which the numerical reflection is small. The good ranges of $R_{\rm th}$ and n are found to be different for different thicknesses of PML. The thicker the PML, the larger the value of n, and the smaller the value of $R_{\rm th}$ should be chosen. From extensive numerical tests, the optimum range of n versus the thickness of PML medium is presented in Fig. 2, and the optimum range of $R_{\rm th}$ versus the PML thickness is shown in Fig. 3. Fig. 3 also shows the range of actual numerical reflection coefficient, at the normal incident of angle, that can be expected when n and $R_{\rm th}$ are chosen within the specified regions shown in Figs. 2 and 3.

C. Time-Marching Schemes in Implementing PML

In Berenger's papers, the exponential time-marching scheme was used in the finite-difference equations for PML [1], [2]. Our tests show no noticeable differences in numerical results obtained by the exponential time-marching scheme and the standard Yee's central difference scheme. Fig. 4 shows the numerical reflection coefficients, at the normal incident angle, of an 8-cell PML implemented with the exponential time-marching scheme and the standard Yee's scheme. The numerical reflection coefficient is obtained by the ratio of the Fourier transformed reflected field and the incident field. In this example, the theoretical reflection coefficients of PML are chosen as 10^{-3} and 10^{-6}, respectively, and the value of power n in (4) is set to 2. As can be seen from Fig. 4, there is virtually no difference in numerical results computed by the exponential time-marching scheme and the standard Yee's scheme. Same observations are obtained in cases where incident waves are not of the normal incident angle.

The reason for the above phenomenon can be explained as follows. Inside the PML medium, fields may vary rapidly in space, but they do not vary any faster in time than they do when PML is absent. Therefore, the selection of the time-marching scheme is not critical and it is not essential to use the exponential time-marching scheme in implementing PML.

III. Numerical Tests of PML Applied toWaveguides

A. Performance of PML for Waveguides

Consider the structure of a parallel-plate waveguide shown in Fig. 5. The separation a between the two metal plates is 40 mm. The lowest order mode of this structure is the TM_0 mode which is actually a TEM mode with a cutoff frequency at dc. The propagation of the TM_0 mode fields along the parallel-plate waveguide is essentially a 1-D wave propagation problem. For absorbing outgoing waves of TM_0 mode, which are of normal incident angle to the free space—PML interface, the PML boundary condition can perform very well in an ultra-wide frequency spectrum, as reported in [4].

The lowest order nonTEM mode in the parallel-plate waveguide is TM_1 and TE_1 modes, which both have a cutoff frequency $f_c = c/2a = 3.75$ GHz. Let us first examine how the PML boundary condition performs for absorbing the TM_1 mode wave. Fig. 6 shows the numerical reflection coefficients versus frequency for 16-cell PML, calculated as the ratio of the reflected wave and the incident wave at the location of free space—PML interface. The theoretical reflection coefficient $R_{\rm th}$ of PML is chosen to be $10^{-4}, 10^{-6}, 10^{-8}$, and 10^{-10}, respectively, and the conductivity profiles of PML are all chosen to be parabolic ($n = 2$). It can be seen from Fig. 6 that the performance of PML for TM_1 mode is quite different from that for TM_0 mode. In the frequency range somewhat above the cutoff frequency, PML performs very well. The numerical reflection reaches its minimum obtainable value when the theoretical reflection coefficient $R_{\rm th}$ is set at about 10^{-6} or below. At the cutoff frequency, as can be observed from Fig. 6, all the reflection coefficients approach to 1. In the frequency range below f_c, where waves are evanescent, it

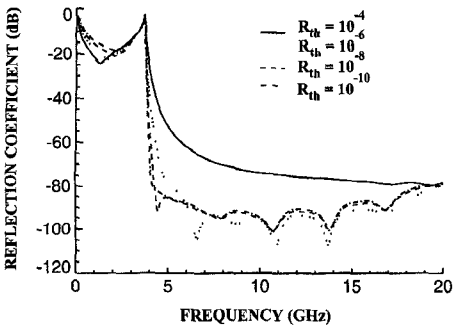

Fig. 6. Numerical reflection coefficients of TM_1 mode for 16-cell PML in the parallel-plate waveguide of Fig. 5, when the theoretical reflection coefficient is set at different values.

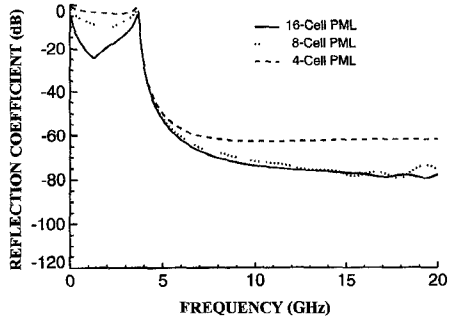

Fig. 7. Numerical reflection coefficients of TM_1 mode in the parallel-plate waveguide of Fig. 5 for PML's of different thicknesses. The theoretical reflection coefficient of PML is set at 10^{-4}.

is clear that the reflection coefficients are significantly larger than those in the frequency range above f_c. These numerical results are consistent with the prediction made in Section II. Fig. 7 displays the reflection coefficients versus frequency for 4-cell, 8-cell, and 16-cell PML's, where the theoretical reflection coefficient is set at 10^{-4} and the conductivity profile is parabolic. Similar conclusions can be obtained from the results in Fig. 7 as those from Fig. 6. In the frequency range below the cutoff, the smaller reflection coefficient for thicker PML medium, seen from Fig. 7, is not due to the absorption of evanescent waves in PML, but is simply due to the original attenuation of the evanescent wave in the longer round path from the free space—PML interface to the electric wall terminating the PML medium. As a matter of fact, PML does not introduce additional attenuation to the evanescent wave, while the spatial variation of conductivity in PML causes additional reflections. As will be shown later, the attenuation of evanescent waves in a section of PML is actually somewhat smaller than that in a section of free space of the same length.

For the structure of the parallel-plate waveguide, it is possible to find analytic solutions of the field in free space and in PML medium. Let us consider the case in which the conductivities (σ, σ^*) of PML are constant with space. For TM_1 mode, it is easy to find that $k\sin\varphi$ and $k\cos\varphi$ in (3) are

$$k\sin\varphi = \pi/a \tag{7}$$

$$k\cos\varphi = \sqrt{\omega^2\mu_0\epsilon_0 - (\pi/a)^2}. \tag{8}$$

By substituting $k\sin\varphi$ and $k\cos\varphi$ in (7) and (8) into (3), one can find that, when frequency f is larger than f_c, the attenuation constant α and the phase constant β are

$$\alpha = \frac{\sigma_x}{\epsilon_0\omega}\sqrt{\omega^2\mu_0\epsilon_0 - (\pi/a)^2} \tag{9}$$

$$\beta = \sqrt{\omega^2\mu_0\epsilon_0 - (\pi/a)^2}. \tag{10}$$

When $f < f_c, k\cos\varphi$ becomes an imaginary number, the attenuation and phase constants can be found as

$$\alpha = \sqrt{(\pi/a)^2 - \omega^2\mu_0\epsilon_0}. \tag{11}$$

$$\beta = -\frac{\sigma_x}{\epsilon_0\omega}\sqrt{(\pi/a)^2 - \omega^2\mu_0\epsilon_0}. \tag{12}$$

Expressions in (9) to (12) give us the following indications:

1) The attenuation constant below the cutoff frequency is exactly the same as that in the waveguide filled with free space. That is, evanescent waves in PML attenuate in the same rate as those in the waveguide filled with free space.
2) The phase constant above the cutoff frequency is exactly the same as that in the waveguide filled with free space. That is, propagating waves in PML travel in the same speed as those in the vacuum-filled waveguide.
3) The attenuation constant above the cutoff frequency is not zero. This is why PML can absorb propagating waves above the cutoff frequency. But as the frequency approaches the cutoff frequency, the attenuation constant α also approaches zero, indicating total reflection at the cutoff frequency.
4) The phase constant below the cutoff frequency is not zero, but is of the "abnormal" negative values.

Analyses above explain why PML is effective for absorbing propagating waves and ineffective for absorbing evanescent waves and waves near the cutoff frequency. It is actually not a difficult task to verify the results in (9) to (12) numerically. By launching a TM_1 mode wave in a waveguide filled with PML, a field component ψ at two locations, x and $x+h$, along the longitudinal direction of the waveguide can be recorded. The attenuation and phase constants of the TM_1 wave in PML can be extracted by following operations

$$\alpha = \frac{1}{h}\ln\left|\frac{\mathcal{F}[\psi(x,t)]}{\mathcal{F}[\psi(x+h,t)]}\right| \tag{13}$$

$$\beta = \frac{1}{h}\mathrm{Im}\left(\ln\frac{\mathcal{F}[\psi(x,t)]}{\mathcal{F}[\psi(x+h,t)]}\right) \tag{14}$$

where $\mathcal{F}$ represents the Fourier transform, Im is the operator of taking the imaginary part of a complex variable. The waveguide for this test is chosen to be long enough so that reflections from end boundaries have not reached the observation points at the time the incident wave is diminished to virtually zero.

Fig. 8 shows the attenuation constant α versus frequency, obtained from numerical computation, expressed in (13), and from theoretical derivations, expressed in (9) and (11). Fig. 9 shows the comparison of numerically and theoretically computed phase constant β versus frequency. The conductivity of PML is constant in space and chosen to be 0.1 S/m. As can be seen from Figs. 8 and 9, theoretical predictions on α and β match very well with numerical solutions.

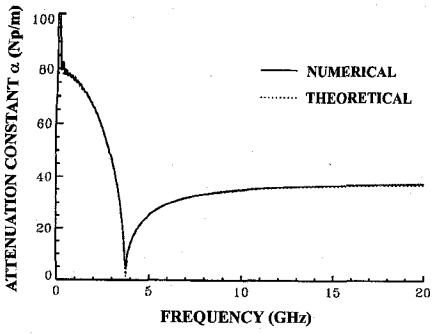

Fig. 8. Attenuation constant in a parallel-plate waveguide filled with PML. The electric conductivity of PML is constant and equal to 0.1 S/m.

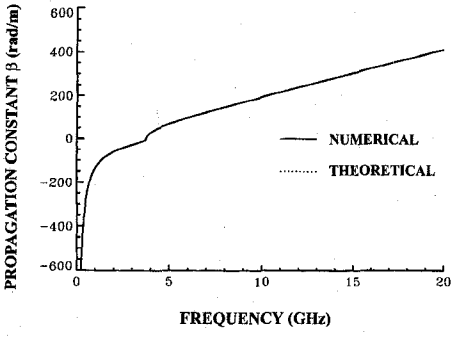

Fig. 9. Phase constant in a parallel-plate waveguide filled with PML. The electric conductivity of PML is constant and equal to 0.1 S/m.

Next, let us look at TE modes of the parallel-plate waveguide. The TE_n mode of the parallel-plate waveguide is actually the same as the TE_{n0} mode of the rectangular waveguide. Fig. 10 displays the numerical reflection coefficients versus frequency for TE_{10}, TE_{20} and TE_{30} modes of a rectangular waveguide, where the PML medium of a parabolic conductivity profile is of 16-cell thick. From Fig. 10, the same conclusions can be made as those for the TM_1 mode of the parallel-plate waveguide. Since higher-order evanescent waves attenuate faster than lower-order ones, reflections of higher-order evanescent waves are consequently smaller.

B. Performance of Higdon's Type of Boundary Condition for Waveguides

As a comparison with PML boundary condition, let us consider Higdon's type of absorbing boundary condition. The principle and analysis of Higdon's boundary condition can be found in [5], [6]. In [7], Higdon's boundary condition is revised to absorb propagating and/or evanescent waves. The general expression of the Higdon's type of boundary condition can be written as

$$\left[\prod_{i=1}^{N}\left(\frac{\partial}{\partial x}+\frac{\cos\varphi_i}{c}\frac{\partial}{\partial t}+\alpha_i\right)\right]\psi=0 \tag{15}$$

where φ_i's and α_i's are parameters. The N_{th}-order boundary condition (15) consists of N first-order boundary operators, each has its parameter (φ_i, α_i).

For a plane wave of an attenuation constant α in the x direction and an incident angle φ, the reflection coefficient of

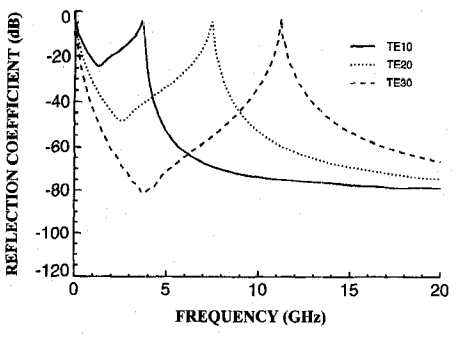

Fig. 10. Reflection coefficients of TE_{10}, TE_{20} and TE_{30} modes in a rectangular waveguide for 16-cell PML with its theoretical reflection coefficient set at 10^{-4}.

the boundary condition (15) can be found to be approximately

$$R\approx-\prod_{i=1}^{N}\frac{(\alpha_i-\alpha)+j\frac{\omega}{c}(\cos\varphi_i-\cos\varphi)}{(\alpha_i+\alpha)+j\frac{\omega}{c}(\cos\varphi_i+\cos\varphi)}. \tag{16}$$

From (16), it can be seen that minimum reflection occurs when α_i is chosen to be α, and φ_i is chosen to be φ. For a certain mode of field in a waveguide, the incident angle φ and the attenuation constant α are frequency dependent. Therefore, one pair of (φ_i, α_i) corresponds to one particular frequency around which the reflection coefficient of the boundary condition is small. If we can select the N pairs of (φ_i, α_i) at proper frequencies, it is possible to have the boundary condition (15) perform well over a very wide frequency spectrum.

Let us consider the TM_1 mode of the parallel-plate waveguide of Fig. 5 again. Fig. 11 shows the reflection coefficient of a fourth-order ($N = 4$) Higdon's boundary condition, where the frequencies of optimum absorption are chosen to be 5, 8, 12, and 16 GHz. Since the frequencies of optimum absorption are all above the cutoff frequency (3.75 GHz), α_i's should be zero. In numerical computations, especially for high-order boundary conditions ($N \geq 3$), a small value of α_i can help maintain the stability of computation [8]. For the results shown in Fig. 11, the α_i's are chosen as follows: $\alpha_1 = 0, \alpha_2 = 0, \alpha_3 = 0.02/dx$ and $\alpha_4 = 0.02/dx$, where dx is the space step of the finite-difference grid. The reflection coefficient shown in Fig. 11 is obtained from the incident and the reflected fields 16 cells away from the outer boundary. Comparison between results of Higdon's boundary condition in Fig. 11 and those of 16-cell PML in Fig. 6 shows that, for propagating waves, the reflection coefficient of a fourth-order Higdon's boundary condition can also reach as low as -100 dB, which is not worse than that of a 16-cell PML. Also notice that, in Fig. 11, the reflection coefficient in the frequency range below f_c is somewhat smaller than those in Fig. 6, although the Higdon's boundary condition for this test is not set to absorb evanescent waves.

Higdon's boundary condition (15) can be set to absorb evanescent waves, as shown in [7]. We can select some boundary operators to absorb propagating waves, while others to absorb evanescent waves. Fig. 12 shows the reflection coefficient for a fifth-order Higdon's boundary condition, where the frequencies of optimum absorption are chosen to be 1, 2.5, 5, 10, and 15 GHz. That is, there are two boundary operators

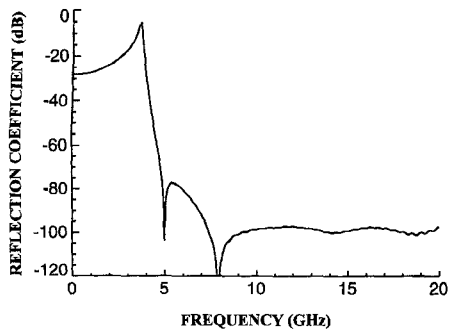

Fig. 11. Reflection coefficient of a fourth-order Higdon's boundary condition with its optimum frequencies of absorption set at 5, 8, 12, and 16 GHz.

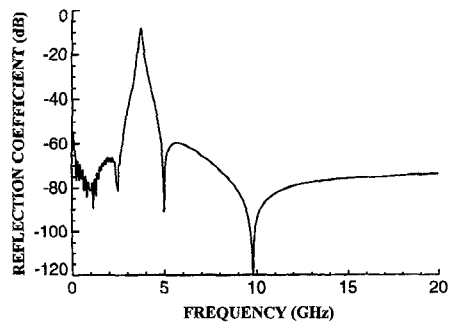

Fig. 12. Reflection coefficient of a fifth-order Higdon's boundary condition with its optimum frequencies of absorption set at 1, 2.5, 5, 10, and 15 GHz.

set for evanescent waves, and three for propagating waves. Corresponding parameters for this boundary condition are: $\alpha_1 = 75.7, \alpha_2 = 58.5, \alpha_3 = 20, \alpha_4 = 0, \alpha_5 = 0$; $\cos\varphi_1 = 0, \cos\varphi_2 = 0, \cos\varphi_3 = 0.968, \cos\varphi_4 = 0.927, \cos\varphi_5 = 0.66$. From Fig. 12, we can see the reflection coefficient for evanescent waves is substantially reduced from that in Fig. 11 and from those corresponding to PML shown in Figs. 6 and 7.

From above comparisons between PML and Higdon's boundary condition, we can find the following advantages and disadvantages of the two boundary conditions. PML can absorb propagating waves very well but not evanescent waves. So PML cannot be placed very close to waveguide discontinuities where evanescent waves are significant. Higdon's boundary condition can be tuned to absorb both evanescent and propagating waves. The selection of parameters of Higdon's boundary condition is geometry and mode dependent, and one needs to pay special attention to numerical stability, while PML does not need much tuning in its implementation.

C. Combination of PML with Higdon's Type of Boundary Condition

From the above discussions, it seems that the combination of PML with Higdon's boundary condition should result in a good absorbing boundary condition for both propagating and evanescent waves. That is, the PML medium is terminated by a Higdon's type of boundary condition instead of by an electric wall. With such a boundary condition, the propagating wave is mostly absorbed by PML, and the evanescent wave is absorbed by the Higdon's boundary condition set for the evanescent wave.

However, the above expectation is not met in numerical tests. Numerical computations show that Higdon's boundary condition for terminating PML can actually do little improvement on absorbing evanescent waves. The reason for this phenomenon can be explained as follows.

For an incident wave expressed in (3) in a PML, the reflection coefficient of Higdon's boundary condition (15) can be found to be approximately

$$R \approx -\prod_{i=1}^{N} \frac{(\alpha_i - \alpha) + j\left(\frac{\omega}{c}\cos\varphi_i - \beta\right)}{(\alpha_i + \alpha) + j\left(\frac{\omega}{c}\cos\varphi_i + \beta\right)}. \tag{17}$$

In order to have small reflection for evanescent waves, parameters α_i's should match the attenuation constant α, and parameters $\omega/c\cos\varphi_i$'s should match the phase constant β. Notice that the phase constant β in PML is of negative values for evanescent waves, as can be seen from (12) and Fig. 9. It is found that the selection of negative values of $\omega/c\cos\varphi_i$ will lead to unstable numerical solutions. So the value of $\omega/c\cos\varphi_i$ that is closest to the value of the phase constant β of evanescent waves is zero. When $\omega/c\cos\varphi_i$'s are set to zero, (17) becomes

$$R \approx -\prod_{i=1}^{N} \frac{(\alpha_i - \alpha) - j\beta}{(\alpha_i + \alpha) + j\beta}. \tag{18}$$

The absolute values of β are typically much larger than those of α. Therefore, even the parameter α_i matches the attenuation constant α, as can be seen from (18), the reflection coefficient R is not to be reduced significantly.

Fig. 13 shows the numerical reflection coefficients of PML terminated by various boundary conditions. The PML medium for this test is of parabolic conductivity profile, 16-cells thick, and a theoretical reflection coefficient of 10^{-4}. The Higdon's boundary conditions terminating PML are all of the first-order. The incident wave considered is the TM_1 mode of the parallel-plate waveguide shown in Fig. 5. Curve 1 in Fig. 13 corresponds to PML terminated by an electric wall. Curve 2 corresponds to PML terminated by a first-order Higdon's boundary condition with α_1 and $\cos\varphi_1$ chosen to be zero. When α_1 and $\cos\varphi_1$ are both equal to zero, the Higdon's boundary condition actually represents a magnetic wall. The location of the magnetic wall is at half-space step away from the terminating boundary, and this is probably the reason why the reflection coefficient of curve 2 is a little larger than that of curve 1. For curve 3 in Fig. 13, the parameter α_1 is chosen to be 58.5, and $\cos\varphi_1$ is zero. The value of α_1 matches the attenuation constant α at the frequency 2.5 GHz. It can be seen that the Higdon's boundary condition terminating PML has little effect, even at 2.5 GHz, in absorbing evanescent waves. For curve 4, parameters α_1 and $\cos\varphi_1$ are chosen to be 704.3 and 0.93, which match the attenuation and phase constants in the PML half-space step to the terminating boundary at the frequency of 10 GHz. As can be seen from Fig. 13, such Higdon's boundary condition can substantially reduce the reflection of propagating waves.

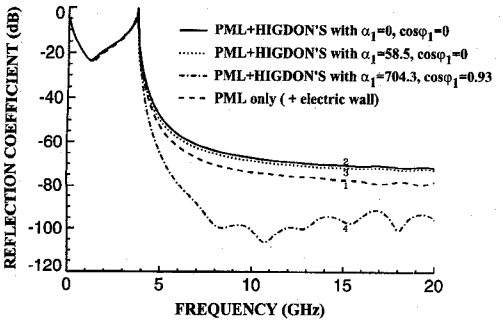

Fig. 13. Reflection coefficients of a 16-cell PML terminated with different boundary conditions.

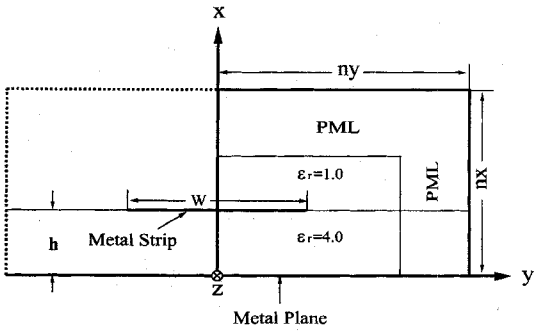

Fig. 14. Cross section of the computation domain for a microstrip line. The width of the metal strip is $W = 1000\ \mu$m. The thickness of the substrate $h = 500\ \mu$m. The space step $\Delta x = \Delta y = \Delta z = 125\ \mu$m. Due to the symmetry of the structure, half of the physical structure is computed.

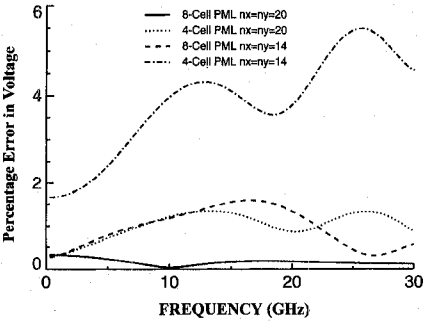

Fig. 15. Percentage errors in the computed voltage of the microstrip line of Fig. 14. The computation domain of the cross section is of 20×20 or 14×14 cells. The thickness of PML is 8 or 4 cells.

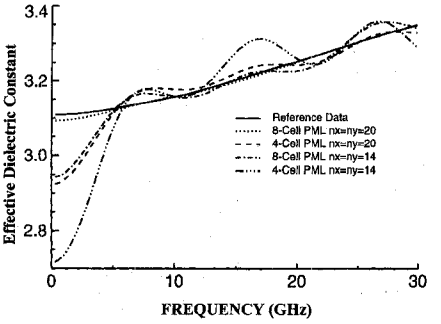

Fig. 16. Numerically computed effective dielectric constant of the microstrip line of Fig. 14. The computation domain of the cross section is of 20 × 20 or 14 × 14 cells. The thickness of PML is 8 or 4 cells.

Numerical results shown above demonstrate that the combination of PML with Higdon's boundary condition can improve the absorption property for propagating waves, but not for evanescent waves.

IV. Numerical Tests of PML Applied to Microstrip Lines

To simulate a wave propagation along a microstrip line, PML is placed near the outer computation domain, as shown in Fig. 14. Due to the symmetry of the structure, only half of the 3-D structure is computed, and the surface at the center of the metal strip is modeled as a magnetic wall. The number of space steps in the transverse cross section of the computation domain nx and ny are denoted in Fig. 14. The relative dielectric constant of the substrate is 4.

At the end surfaces perpendicular to the metal strip, where outgoing waves incident upon outer boundaries in near normal incident angles, PML works very well as expected. A 16-cell PML can make the reflection coefficient as low as -80 dB. On the top and the side surfaces of the computation domain, where fields are mostly evanescent in the direction normal to outer surfaces and propagating wave components are incident upon outer boundaries with grazing angles, PML is found to be less effective.

Fig. 15 shows the percentage errors in the computed voltage of the microstrip line for different thicknesses of the PML placed at different distances away from the center of the metal strip. Computation domains in the transverse direction $(nx \times ny)$ for the results shown in Fig. 15 are 14×14 and 20×20. The percentage errors in the voltage of the microstrip line is calculated with respect to the reference voltage obtained with a very large computation domain. The large computation domain is of the size $nx \times ny = 210 \times 80$, and terminated by a fourth-order Higdon's boundary condition. Fig. 16 is the corresponding computed effective dielectric constant ϵ_{reff} of the microstrip line for PML's of different thicknesses and distances to the center of the metal strip. ϵ_{reff} is calculated from the Fourier transform of voltages at two locations along the microstrip line [9]. In Fig. 16, the curve for the 8-cell PML and for $nx \times ny = 20 \times 20$ almost coincides with the one computed with the large computation domain, while other curves contain substantial errors. It can be seen from Figs. 15 and 16 that PML in general can be used for the simulation of wave propagation along microstrip structures, but needs to be placed at a certain distance away from the metal strip and of enough thickness to ensure the reliability of the computed electrical properties.

V. Conclusion

This paper presents the numerical implementation and performance of perfectly matched layer boundary condition for modeling wave propagation in waveguide structures. It is shown theoretically and numerically that PML is very effective in absorbing propagating waves and ineffective in absorbing evanescent waves. The combination of PML with Higdon's boundary condition can enhance the absorption property for propagating waves but not for evanescent waves. In modeling

wave propagations in waveguide structures, PML needs to be placed at certain distance away from modeled structures where evanescent waves are significant.

In our most recent work, a modified formulation of the perfectly matched layer is derived. This new boundary condition, which we call the generalized perfectly matched layer (GPML) is found to be able to effectively absorb both propagating and evanescent waves and perfectly match nonPML lossy media [10].

REFERENCES

[1] J. P. Berenger, "A perfectly matched layer for the absorption of electromagnetic waves," *J. Comput. Physics*, 114, pp. 185–200, Oct. 1994.

[2] ——, "A perfectly matched layer for free-space simulation in finite-difference computer codes," presented at *Euro. Electromagnetics 94*, Bordeaux, France, May 30–June 4, 1994.

[3] D. S. Katz, E. T. Thiele, and A. Taflove, "Validation and extension to three dimensions of the Berenger PML absorbing boundary condition for FD-TD meshes," *IEEE Microwave Guided Wave Lett.*, vol. 4, no. 8, pp. 268–270, Aug. 1994.

[4] C. E. Reuter, R. M. Joseph, E. T. Thiele, D. S. Katz, and A. Taflove, "Ultrawideband absorbing boundary condition for termination of waveguiding structures in FD-TD simulations," *IEEE Microwave Guided Wave Lett.*, vol. 4, no. 10, pp. 344–346, Oct. 1994.

[5] R. L. Higdon, "Absorbing boundary conditions for difference approximations to the multi-dimensional wave equations," *Math. Comput.*, vol. 47, no. 176, pp. 437–459, Oct. 1986.

[6] ——, "Radiation boundary conditions for elastic wave propagation," *SIAM, J. Numer. Anal.*, vol. 27, no. 4, pp. 831–870, Aug. 1990.

[7] J. Fang, "Absorbing boundary conditions applied to model wave propagation in microwave integrated-circuits," *IEEE Trans. Microwave Theory Tech.*, vol. 42, pp. 1506–1513, Aug. 1994.

[8] ——, "Investigation on the stability of absorbing boundary conditions for the time-domain finite-difference method," in *Proc. 1992 IEEE AP-S/URSI Internat. Symp.*, Chicago, July 18–25, 1992, pp. 548–551.

[9] X. Zhang, J. Fang, K. K. Mei, and Y. Liu, "Calculation of the dispersive characteristics of microstips by the time-domain finite-difference method," *IEEE Trans. Microwave Theory Tech.*, vol. MTT-36, pp. 263–267, Feb. 1988.

[10] J. Fang and Z. Wu, "Generalized perfectly matched layer—An extension of Berenger's perfectly matched layer boundary condition," accepted for publication in *IEEE Microwave Guided Wave Lett.*, Dec. 1995.

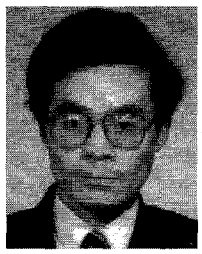

Zhonghua Wu was born in Jiangsu, P. R. China, in 1966. He received the B.S. degree from the University of Science and Technology of China in 1989 and the M.S. degree from the Institute of Geophysics, Chinese Academy of Science, in 1992, both in geophysics. Currently, he is pursuing the Ph.D. degree at the Department of Electrical Engineering, State University of New York at Binghamton.

His research interests include computational electromagnetism, transmission line theory, electrical performance of electronics packaging, CAD, and communications.

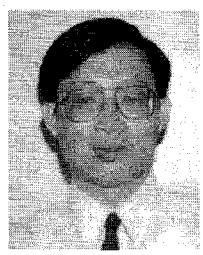

Jiayuan Fang (S'85–M'89) received the M.S. and Ph.D. degrees in electrical engineering from the University of California at Berkeley in 1987 and 1989, respectively.

He was an Assistant Professor from 1990 to 1994, and is currently an Associate Professor, in the Department of Electrical Engineering at the State University of New York at Binghamton. His research interests are in applied electromagnetics, numerical methods, and electromagnetic modeling and simulation of electronic packaging.

Dr. Fang has been an Associate Editor of IEEE TRANSACTIONS ON COMPONENTS, PACKAGING, AND MANUFACTURING TECHNOLOGY/PART B: ADVANCED PACKAGING since 1994. He received the National Science Foundation Research Initiation Award (RIA) in 1991 and Young Investigator Award (NYI) in 1993.